Langmuir
Letter

pubs.acs.org/Langmuir

Water-Swelling-Induced Morphological Instability of a Supported Polymethyl Methacrylate Thin Film

Benxin Jing† and Jiang Zhao*

Beijing National Laboratory of Molecular Science, Joint Laboratory of Polymer Sciences and Materials, Institute of Chemistry, Chinese Academy of Sciences, Beijing 100190, China

Yan Wang, Xin Yi, and Huiling Duan*

State Key Laboratory for Turbulence and Complex Systems, CAPT, Department of Mechanics and Aerospace Engineering, College of Engineering, Peking University, Beijing 100871, China. †Also affiliated with the Graduate School of the Chinese Academy of Sciences

Received January 30, 2010. Revised Manuscript Received April 23, 2010

The instability of supported poly(methyl methacrylate) (PMMA) thin films in water has been investigated. It is found that PMMA films partially detach from the solid substrate, resulting in the formation of bubbles under water. The process is reversible. Surface morphology analysis shows that the radius of curvature of the bubbles is dependent on the thickness of the PMMA films and is independent of the treatment of the films, such as the annealing temperature and the annealing time. Theoretical analysis based on a two-layer model (the swollen layer and the interior layer) shows that the partial swelling of PMMA in water is the physical origin of bubble formation.

Introduction

The stability of ultrathin polymer films has continuously attracted attention for decades because of the popular application of these systems in coating technology, the microelectronics industry, biomedical devices, and emerging nanotechnology. Frequently, these films are found to be unstable because of the mismatch of physical properties in the layers of films, such as the wettability, thermoexpansion rate, Poisson ratio, and so forth. In many cases, the supported ultrathin polymer films can undergo morphological variations under external stimuli, such as stress, heat, light radiation, and solvent vapor. The instabilities may be exhibited in various forms, such as buckling, wrinkling, fracturing,[1] and dewetting.[2] The instability of a supported polymer film would result in the failure of the polymer film, manifested in fracturing, irrecoverable deformation, and so forth. However, the instability could be used to investigate the properties of supported ultrathin polymer films, including mechanical properties,[3,4] viscoelasticity,[5,6] hydrodynamics and rheology,[7−10] adhesion and failure,[11−14] residual stress,[15,16] and the surface properties of substrates,[17−20] and to create micropatterns[21−24] and nanopatterns.[25−29] In short, the instability of supported polymer films is an excellent tool for investigation in polymer science.

Polymer films are used not only in air but also in nonsolvents or poor solvents in many cases, such as in coatings on boats and microfluidics and nanofluidics in water and other solvents. At present, to our knowledge, there are only a few literature reports on the unstable phenomena of polymer films in nonsolvents, such

*Corresponding authors. E-mail: jzhao@iccas.ac.cn (J.Z.); hlduan@pku.edu.cn (H.D.).

(1) Hutchinson, J. W.; Thouless, M. D.; Liniger, E. G. *Acta Metall. Mater.* **1992**, *40*, 295–308.
(2) Reiter, G. *Phys. Rev. Lett.* **1992**, *68*, 75–78.
(3) Stafford, C. M.; Vogt, B. D.; Harrison, C.; Julthongpiput, D.; Huang, R. *Macromolecules* **2006**, *39*, 5095–5099.
(4) Stafford, C. M.; Harrison, C.; Beers, K. L.; Karim, A.; Amis, E. J.; Vanlandingham, M. R.; Kim, H. C.; Volksen, W.; Miller, R. D.; Simonyi, E. E. *Nat. Mater.* **2004**, *3*, 545–550.
(5) Bodiguel, H.; Fretigny, C. *Macromolecules* **2007**, *40*, 7291–7298.
(6) Gabriele, S.; Damman, P.; Sclavons, S.; Desprez, S.; Coppee, S.; Reiter, G.; Hamieh, M.; Al Akhrass, S.; Vilmin, T.; Raphael, E. *J. Polym. Sci., Part B: Polym. Phys.* **2006**, *44*, 3022–3030.
(7) Bodiguel, H.; Fretigny, C. *Phys. Rev. Lett.* **2006**, *97*, 266105.
(8) Blossey, R.; Munch, A.; Rauscher, M.; Wagner, B. *Eur. Phys. J. E* **2006**, *20*, 267–271.
(9) Fetzer, R.; Rauscher, M.; Seemann, R.; Jacobs, K.; Mecke, K. *Phys. Rev. Lett.* **2007**, *99*, 114503.
(10) Fetzer, R.; Munch, A.; Wagner, B.; Rauscher, M.; Jacobs, K. *Langmuir* **2007**, *23*, 10559–10566.
(11) Cotterell, B.; Chen, Z. *Fracture Strength Solids, Pts 1 and 2* **2000**, *183−187*, 187–192.
(12) Figiel, L.; Lauke, B. *Int. J. Fract.* **2006**, *139*, 71–89.
(13) Fedorov, A.; De Hosson, J. T. M. *J. Appl. Phys.* **2005**, *97*, 123510.
(14) Fedorov, A. V.; van Tijum, R.; Vellinga, W. P.; De Hosson, J. T. M. *Prog. Org. Coat.* **2007**, *58*, 180–186.
(15) Damman, P.; Gabriele, S.; Coppee, S.; Desprez, S.; Villers, D.; Vilmin, T.; Raphael, E.; Hamieh, M.; Akhrass, S. A.; Reiter, G. *Phys. Rev. Lett.* **2007**, *99*, 036101.
(16) Akhrass, S. A.; Reiter, G.; Hou, S. Y.; Yang, M. H.; Chang, Y. L.; Chang, F. C.; Wang, C. F.; Yang, A. C. M. *Phys. Rev. Lett.* **2008**, *100*, 178301.
(17) Kao, J. C. T.; Golovin, A. A.; Davis, S. H. *J. Colloid Interface Sci.* **2006**, *303*, 532–545.
(18) Verma, R.; Sharma, A. *Ind. Eng. Chem. Res.* **2007**, *46*, 3108–3118.
(19) Hamieh, M.; Al Akhrass, S.; Hamieh, T.; Damman, P.; Gabriele, S.; Vilmin, T.; Raphael, E.; Reiter, G. *J. Adhes.* **2007**, *83*, 367–381.
(20) Huang, R.; Stafford, C. M.; Vogt, B. D. *J. Aerosp. Eng* **2007**, *20*, 38–44.
(21) Edmondson, S.; Frieda, K.; Comrie, J. E.; Onck, P. R.; Huck, W. T. S. *Adv. Mater.* **2006**, *18*, 724–728.
(22) Cai, Y.; Newby, B. M. Z. *Langmuir* **2008**, *24*, 5202–5208.
(23) Baralia, G. G.; Filiatre, C.; Nysten, B.; Jonas, A. M. *Adv. Mater.* **2007**, *19*, 4453–4459.
(24) Baffoun, A.; Haidara, H.; Dupuis, D.; Viallier, P. *Langmuir* **2007**, *23*, 9447–9454.
(25) Lin, Y. H.; Jiang, C.; Xu, J.; Lin, Z. Q.; Tsukruk, V. V. *Adv. Mater.* **2007**, *19*, 3827–3832.
(26) Suh, K. Y.; Seo, S. M.; Yoo, P. J.; Lee, H. H. *J. Chem. Phys.* **2006**, *124*, 024710.
(27) Chan, E. P.; Crosby, A. J. *Soft Matter* **2006**, *2*, 324–328.
(28) Mukherjee, R.; Gonuguntla, M.; Sharma, A. *J. Nanosci. Nanotech.* **2007**, *7*, 2069–2075.
(29) Ferrell, N.; Hansford, D. *Macromol. Rapid Commun.* **2007**, *28*, 966–971.

as bumps[30,31] and dewetting.[32−35] Poly(methyl methacrylate) (PMMA) is believed to be a versatile material with potential applications in biomedical fields as well as in novel fluidic devices with small dimensions. The behavior of this material in contact with aqueous solution has been considered to be an important topic. Recently, there has been quite a lot of attention paid to the behavior of the PMMA thin film in water because of its biomedical applications.[36,37] As a poor solvent for PMMA, water has been found to have a great influence on many properties of bulk PMMA such as mechanical properties,[38,39] optical properties,[40] electrical properties,[41,42] the glass transition,[43] and so forth. Because of its sensitivity to water, PMMA was even used to prepare a humidity sensor.[41] Furthermore, an interesting phenomenon was discovered in which a PMMA ultrathin film can be partially swelled in water.[44] It was also found that spin-cast or Langmuir−Blodgett (LB) films of PMMA are poor barriers to water vapor and to liquid water.[45] Thus it is noteworthy to investigate the instability of PMMA films in water.

In this letter, we adopt various microscopy techniques to study the morphological evolution of thin films of PMMA in water, such as the in situ measurement of the film evolution conducted by atomic force microscopy (AFM) and optical microscopy. Moreover, the continuum model has been presented to analyze the physical origin of the morphological evolution of the PMMA film.

Experimental Section

Materials. Monodisperse PMMA with over 79% syndiotactic content (M_w = 21.4 and 56 kg/mol, polydispersity index = 1.07 and 1.08, and T_g = 121.7 and 116.2 °C determined by differential scanning calorimetry) was purchased from Polymer Source Inc. *N*,*N*-Dimethylaminopropyltrimethoxysilane (DMAPS) was purchased from Sigma-Aldrich.

Fabrication of Substrates and Supported PMMA Films. Silicon wafers were used as substrates. To tune the interaction between the substrate and PMMA film, the substrates were chemically modified to be rich in silanol groups or were coated with self-assembled monolayers to be rich in tertiary amino groups on their surfaces. Silicon wafers were first treated with oxygen plasma for 30 min and with piranha solution (3:1 v/v H_2SO_4/H_2O_2) at 120 °C for 1 h to obtain a high surface concentration of silanol groups. (***Caution!*** *Piranha solution is extremely corrosive, and one should be careful when handling it.*) Before spin-casting with PMMA solution, the silicon wafers were heated to 130 °C in vacuum for 2 h to remove the water on their surfaces (so-called "dehydrated" in the following text).

Silica surfaces rich in tertiary amines were fabricated by functionalizing silicon wafers with DMAPS. The silanol-group-rich silicon wafers were submerged in a solution of DMAPS in anhydrous cyclohexane (1.5 mg/mL) under ambient conditions for 30 min. Then the wafers were rinsed with cyclohexane, ethanol, and deionized water and sonicated for 10 min. After sonication, the wafers were rinsed with deionized water once again and dried in a flow of N_2. The wafers were surface functionalized by tertiary amines, and their surfaces were very smooth (the rms roughness measured by AFM was 0.326 nm). Before the spin-casting, the tertiary amino-silicon wafers were also heated to 130 °C in vacuum for 2 h to dehydrate them.

A PMMA solution in tetrahydrofuran was deposited on the substrates by spin-casting at a speed of 4000 rpm to obtain the supported PMMA films. After fabrication, the supported PMMA films were annealed at different temperatures in vacuum for different lengths of time. Also, control experiments with films deposited on substrates without the dehydration treatment were conducted.

Microscopy. Tapping-mode AFM images were obtained as soon as possible after water was added to the PMMA films on a NanoScope IIIA multimode AFM (Digital Instruments). All of the measurements were conducted under ambient conditions. The thickness of the PMMA films was determined by AFM after being scratched with a blade. Optical microscopy measurements were conducted on an inverted microscope (Olympus IX-71) equipped with a CCD camera (Andor DV887).

Results and Discussion

The PMMA film was unstable when it was immersed in water. Under an optical microscope, circular features were observed to appear and grow in size. An in situ AFM measurement of the sample in water showed that the films detached from the substrate to form bubbles (Figure 1a). In general, the bubbles appeared and grew slowly after water was added. AFM images clearly show the time evolution of the bubble, and typical images are provided in the Supporting Information. Once water was removed, the bubbles disappeared in several minutes, the PMMA films again became flat and smooth, and the morphology before water addition was recovered. The typical section profile of a single bubble is shown in Figure 1b. The profile can be well fit by a spherical cap model, its dimensions can be characterized by its height h and footprint diameter L, and the radius of curvature R of the bubble can be fit from these data.

The typical dimensions of the bubbles and a typical time-evolution curve are shown in Figure 2. The inset of Figure 2a shows the enlargement of a typical bubble with time and the saturation of its growth with prolonged soaking. The data of 21 typical bubbles with a film thickness (d) of 47 nm are displayed in Figure 2a. The measurements show that the h value of each bubble increases with its L value, but the fitting of h and L using a spherical cap model demonstrates a constant value of the radius of curvature, R (~3.3 μm). Moreover, R for all bubbles investigated does not change with time evolution, as shown in Figure 2b in which the solid line is obtained from the theoretical prediction under the assumption of a spherical cap.

The formation of bubbles in PMMA films under water is a phenomenon related to the film properties. Experiments were conducted with films at different annealing times, different annealing temperatures, and different film−substrate interactions. The data are provided in the Supporting Information, in which the dimensions (L and h) of bubbles formed in films under different treatments or surface interactions are displayed. The

(30) Stevens, F.; Leach, R. N.; Langford, S. C.; Dickinson, J. T. *Langmuir* **2006**, *22*, 3320–3325.
(31) Leach, R. N.; Stevens, F.; Seiler, C.; Langford, S. C.; Dickinson, J. T. *Langmuir* **2003**, *19*, 10225–10232.
(32) Bonaccurso, E.; Butt, H. J.; Franz, V.; Graf, K.; Kappl, M.; Loi, S.; Niesenhaus, B.; Chemnitz, S.; Bohm, M.; Petrova, B.; Jonas, U.; Spiess, H. W. *Langmuir* **2002**, *18*, 8056–8061.
(33) Castro, L. B. R.; Almeida, A. T.; Petri, D. F. S. *Langmuir* **2004**, *20*, 7610–7615.
(34) Xu, L.; Shi, T. F.; An, L. *Langmuir* **2007**, *23*, 9282–9286.
(35) Haidara, H.; Vonna, L.; Schultz, J. *Langmuir* **1998**, *14*, 3425–3434.
(36) Castner, D. G.; Ratner, B. D. *Surf. Sci.* **2002**, *500*, 28–60.
(37) Ko, H. S.; Liu, C. W.; Gau, C. *J. Micromech. Microeng.* **2007**, *17*, 1640–1648.
(38) Ishiyama, C.; Higo, Y. *J. Polym. Sci., Part B: Polym. Phys.* **2002**, *40*, 460–465.
(39) Hamouda, A. M. S. *J. Mater. Process. Technol.* **2002**, *124*, 238–243.
(40) Watanabe, T.; Ooba, N.; Hida, Y.; Hikita, M. *Appl. Phys. Lett.* **1998**, *72*, 1533–1535.
(41) Matsuguchi, M.; Sadaoka, Y.; Sakai, Y.; Kuroiwa, T.; Ito, A. *J. Electrochem. Soc.* **1991**, *138*, 1862–1865.
(42) Cui, L. L.; Jiang, J.; Xia, Z. G.; Chen, G. J.; Wang, Z. Z. *J. Electrost.* **1998**, *44*, 61–65.
(43) Smith, L. S. A.; Schmitz, V. *Polymer* **1988**, *29*, 1871–1878.
(44) Tanaka, K.; Fujii, Y.; Atarashi, H.; Akabori, K. i.; Hino, M.; Nagamura, T. *Langmuir* **2008**, *24*, 296–301.
(45) Sutandar, P.; Ahn, D. J.; Franses, E. I. *Macromolecules* **1994**, *27*, 7316–7328.

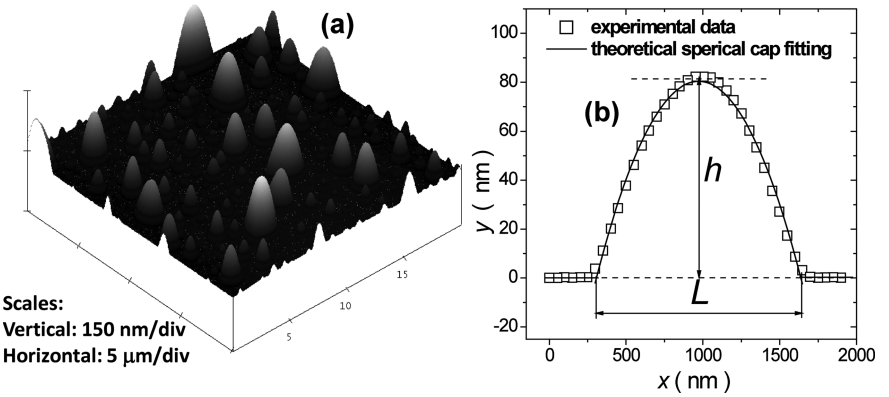

Figure 1. (a) AFM image ($20 \times 20\ \mu m^2$) of PMMA ($M_w = 21.4$ kg/mol) bubbles after 186 min of being soaked in water. (b) Typical section profile of the bubbles. The profile was fit by a spherical cap model, demonstrated by the solid line. The film was deposited via spin-casting onto the dehydrated DMAPS substrate and annealed at 120 °C in vacuum for 24 h. The thickness of the PMMA film is 47 nm.

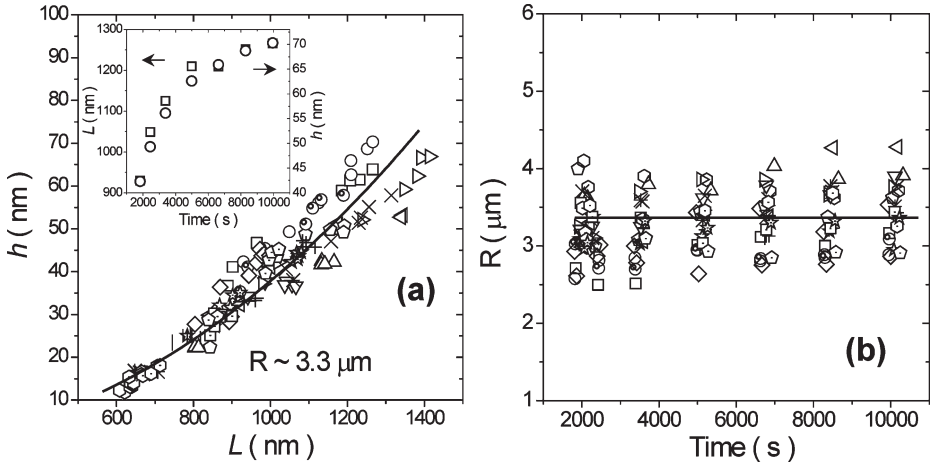

Figure 2. (a) Dimension data of 21 bubbles (h and L) in PMMA films at different observation times. The solid line demonstrates the fitting of the radius of curvature (R) using the model of a spherical cap for the bubbles. (Inset) Time evolution of the dimension of a typical bubble. (b) Time evolution of the radius of curvature (R) of the bubble. Each series of symbols corresponds to a specific bubble. Data are sampled with 21 bubbles in total and different water-soaking times. The solid line demonstrates the results of the data fitting ($R \approx 3.3\ \mu m$). The film was deposited via spin-casting on a dehydrated DMAPS substrate and annealed at 120 °C in vacuum for 24 h. The thickness of the PMMA film is 47 nm.

data show that the radius of curvature is independent of the conditions used for film treatment and surface chemistry. However, these conditions did affect the kinetics of bubble formation. Qualitatively, the longer the annealing time and the higher the annealing temperature, the more slowly the bubbles grow. When the PMMA films were annealed above their glass-transition temperature, for example, at 160 °C, bubble formation was hardly observed during the observation time. If the interaction between the film and the substrate was weak, for example, when the substrate surface was not dehydrated, then the growth of PMMA bubbles was so fast that its kinetics could not be followed by AFM measurements. These results indicate that the kinetics of bubble formation relies heavily on the interaction between the film and the substrate because the longer the annealing time and the higher the annealing temperature, the more the dehydration treatment of the substrate enhances such an interaction. This fact is further confirmed by image analysis, showing that with increasing annealing temperature the average footprint area of each bubble decreases, although the number of bubbles increases. This result indicates that the annealing at higher temperature promotes an interaction between the substrate and the film so that more pinning sites are generated (Supporting Information).

From the analysis above, we know that the radius of curvature of the bubbles is independent of the conditions used for film treatment and surface chemistry and depends only on the film thickness. Systematic experiments were conducted with PMMA films with different original thicknesses. (The film thickness was measured in air by AFM after the sample was scratched with a blade.) The data are provided in Figure 3a, showing the dimensions of the bubbles with different film thicknesses (d). By fitting these data using a spherical cap model, the data show that the radius of curvature of the bubbles increases monotonously with the film thickness (Figure 3b). These facts indicate that the morphology of the bubbles is affected only by the original thickness of the film.

What is the physical origin of this kind of bubble formation? A supported elastic film will partially detach from the substrate when the compressive stress in the film is high enough.[1] The compressive stress might come from the mismatch in the film such as an expansion coefficient due to heat or solvent. If the compressive stress is equibiaxial, then the buckling morphology will be a blister or bubble.[1] In this study, two possible mechanisms are considered for the formation of PMMA bubbles: one is the interfacial tension between water and PMMA, and the other is the swelling of the PMMA film in water. The lowered interfacial tension of water/PMMA compared with that of the original air/PMMA interface should favor more surface area. However, because PMMA is rather rigid at room temperature, this factor

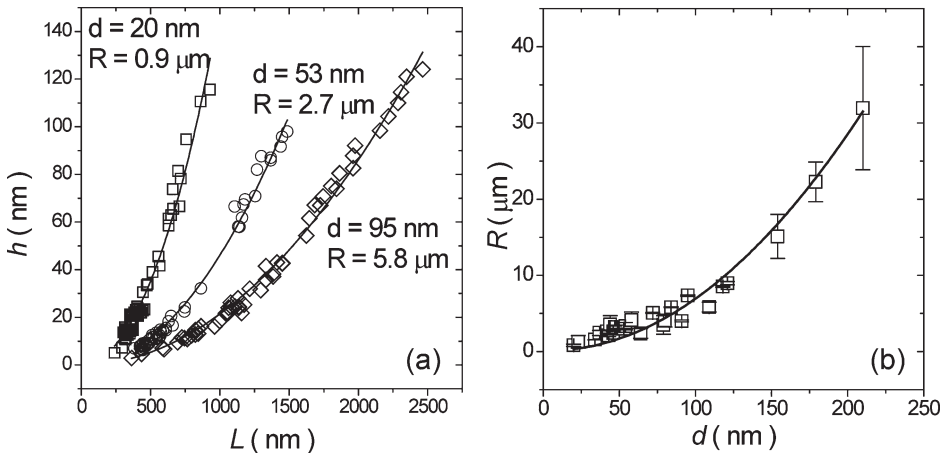

Figure 3. (a) Dimensions of the bubbles on a PMMA film with three different thicknesses: 20 (□), 53 (○), and 95 nm (△). The solid line denotes the fitting curve based on the theoretical model. (b) Radius of curvature of the bubbles as a function of the original thicknesses of the PMMA films. The solid line is obtained from the theoretical model.

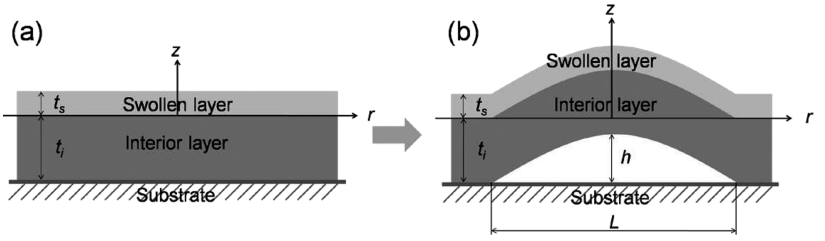

Figure 4. Sketch of the supported PMMA film and its deformation process upon water adsorption: (a) layer formation immediately after water swelling and (b) layer deformation after water swelling for a longer period of time.

is believed to have a minor effect, which is also proven by further theoretical analysis given below. The second mechanism sounds reasonable, and there have been experimental reports about it. For example, Tanaka et al. observed the nonuniform swelling phenomena of a PMMA film under water by neutron reflectivity measurments.[44] They found that, when in contact with water, PMMA is partially swollen and the film can be modeled as consisting of a swollen layer and an interior layer that is not in contact with water. In the current case, the swelling makes the swollen layer expand more than the interior layer. As a consequence, a mismatch between the swollen layer and the interior layer builds up and induces bubble formation in the film. To discriminate between these two mechanisms, a theoretical analysis has been conducted.

Theoretical Analysis

To understand the physical origin of bubble formation, the question of what is in the bubble (water, air, or vacuum) should be answered first. However, this question is difficult to answer only by the present experiment. On the basis of the following two arguments, we believe that the space inside the bubbles is filled with air. First, a previous study show that the PMMA thin film has good gas permeability and that nitrogen and oxygen can pass through the PMMA film within a very short time (e.g., a few microsecond).[46] This can easily allow the residual air in water to pass through the PMMA film. Second, the results of the theoretical model with the consideration of the presence of air matche the experiment data well. (Please refer to later text.) According to the nonuniform swelling phenomena observed by Tanaka et al., the supported PMMA film in water can be modeled as two layers: a swollen layer next to water and an interior layer away from water and next to the substrate (c.f., Figure 4a,b).[44] On the basis of this two-layer model, the misfit strain (ε^*) between the swollen layer (thickness t_s) and the interior layer (thickness t_i) contributes to the deformation of the PMMA film (swollen layer + interior layer) whereas the interfacial tension (a_u for the upper surface and a_l for the lower interface) between water and film plays a role as well.

When the top layer in the PMMA film adsorbs water, misfit strain will be induced between the swollen and interior layers. Here, with the small deformation assumption, the strain (ε) in the bending direction is considered to be a function of the z coordinate (Figure 4b) and the strain compatibility equations result in a linear relation between ε and the bending curvature (κ). The strain can be expressed as

$$\varepsilon = (z - z_0)\kappa \tag{1}$$

in which $-t_i \le z \le t_s$ and z_0 denotes the position of the bending axis, which is defined as the line where the bending strain component is zero. κ is the curvature defined as the inverse of the radius of curvature of the bending axis. Because the shape of the bubble is a spherical cap (Figure 1b), we have $\kappa = R^{-1}$. The elastic stresses (σ_s and σ_i) in the swollen layer and the interior layer can be obtained from Hooke's law and can be expressed as $\sigma_s = E_s(\varepsilon_s - \varepsilon^*)$ and $\sigma_i = E_i\varepsilon_i$, where E is the Young's modulus and subscripts s and i identify the quantities related to the swollen

(46) Hu, C.-C.; Fu, Y.-J.; Lee, K.-R.; Ruaan, R.-C.; Lai, J.-Y. *Polymer* **2009**, *50*, 5308–5313By adopting the data in this reference, the mass flow through a 46 nm-thick PMMA film is calculated to be 5.1×10^{-6} m^3/s, and the time for air to fill a bubble of typical dimension (L = 1 μm, h = 53 nm) is about 5 ms.

layer and interior layer, respectively. Here, the 1D model is used for simplicity, but this approach also holds for the 2D condition. Compared with the initial planar state, the change in the bending moment due to buckling will be[47]

$$\Delta M = \int_0^{t_s} \sigma_s(z - z_0)\, dz + \int_{-t_i}^{0} \sigma_i(z - z_0)\, dz + a_u(t_s - z_0) - a_l(t_i + z_0) = -B\kappa \quad (2)$$

where B is the bending stiffness,[47]

$$B = \frac{E_i}{3}[(h+t_i - z_0)^3 - (h - z_0)^3] + \frac{E_s}{3}[(h+t_i+t_s - z_0)^3 - (h+t_s - z_0)^3] \quad (3)$$

By solving the equations above, the curvature κ can be obtained. The curvature, which is induced by the misfit strain, is expressed as

$$\kappa = \frac{3}{t_i} \frac{\alpha\beta(\beta+1)\varepsilon^* + \left\{ \frac{a_l}{t_i E_i}[\alpha\beta(2+\beta)+1] - \frac{a_u}{t_i E_i}[(1+2\beta)+\alpha\beta^2] \right\}}{\alpha^2\beta^4 + 1 + 2\alpha\beta(2+3\beta+2\beta^2)} \quad (4)$$

where $\alpha = E_s/E_i$ and $\beta = t_s/t_i$. The expression clearly shows that κ is a function of the thicknesses of the swollen layer and the interior layer, the Young's modulus of the layers, and the interfacial tension. The thickness (t_s = 11 nm) of the swollen layer is adopted from Tanaka's work.[44] An average value of the Young's modulus of the swollen layer is taken as 2.0 GPa. The values of the interfacial tension of the upper surface (a_u) and lower interface (a_l) are adopted as 18.1 and 38.5 mN/m, respectively.[48] It should be noted that for all film thicknesses, using the data above, the value of the bubble curvature due to misfit (the first term in eq 4) is larger than that due to the interfacial tension: the former is 20 times larger than the latter, and there is no difference in bubble curvature with and without interfacial tension. This fact indicates that the influence of interfacial tension can be neglected. Therefore, we will focus only on the misfit contribution (ε^*). First, we get the misfit strain ε^* from the data in Figure 2b (d = 47 nm, R = 3.3 μm), and the value of misfit ε^* = 0.045 can be obtained by eq 4. Assuming that the misfit is the same for all swollen films, the radii of curvature of bubbles can be calculated via eq 4. The result is shown in Figure 3b (as the solid line), demonstrating excellent agreement with the experimental data.

Two alternate models have been considered regarding the substances inside bubbles. One model assumes that the inside of the bubble is water, and a three-layer model is used. The other model considers vacuum inside bubble, and air pressure exerted on the bubbles is considered. Neither of these models provided good enough agreement with the experimental data, and this gives further support to the assumption of the existence of air inside the bubble. (Details of these analyses are provided in the Supporting Information.)

From the experimental and theoretical analyses, we obtain the following physical origin of bubble formation in a thin PMMA film: when PMMA is in contact with liquid water, a small amount of water is absorbed by PMMA and, as a result, the top layer is swollen. This swollen layer expands and results in the partial detachment of supported PMMA films from substrates, as observed by AFM measurements. The adsorbed water induces a misfit strain between the swollen layer and the interior layer, and this strain causes an equibiaxial compressive stress inside the film. These kinds of stress and misfit strain induce the bending of the PMMA film, and when it exceeds the binding strength between the PMMA film and substrate, film detachment happens. Therefore, the water-swollen induced misfit is the physical origin of bubble formation in thin PMMA films.

Conclusions

Various in situ microscopy techniques, including atomic force microscopy and optical microscopy, have been used to study the morphological evolution of thin films of PMMA in water. Bubble formation was found when the PMMA film was in contact with water; moreover, the continuum model has been presented to analyze the physical origin of the morphological evolution of the PMMA film. Both experiments and theoretical analysis demonstrate that the deformation of the PMMA film mainly depends on the film thickness and Young's modulus. The theoretical and experimental results agrees well, and this shows that the water-swollen induced misfit is the physical origin of bubble formation in thin PMMA films.

Acknowledgment. B.J. and J.Z. acknowledge financial support from the National Natural Foundation of China (NSFC) (under grant nos. 20574080, 50730007, and 20925416). Y.W. and H.D. acknowledge financial support from the NSFC (under grant nos. 10525209 and 10872003), the Foundation for the Author of National Excellent Doctoral Dissertation of PR China (FANEDD, under grant no. 2007B2), research funds for the New Teacher Program (under grant no. 200800011011), and for the Returned Overseas Chinese Scholars of the State Education Ministry of China.

Supporting Information Available: Time evolution of PMMA bubbles in water. Effect of treatment on the morphology of the PMMA film in water. Effect of annealing temperature on the number of bubbles and area. Theoretical analysis of whether water or vacuum is in the bubble. This material is available free of charge via the Internet at http://pubs.acs.org.

(47) Choi, S. R.; Hutchinson, J. W.; Evans, A. G. *Mech. Mater.* **1999**, *31*, 431–447.
(48) Kwok, D. Y.; Wu, R.; Li, A.; Neumann, A. W. *J. Adhes. Sci. Technol.* **2000**, *14*, 719–743.

Supporting Information

Benxin Jing et al, "Water Swelling Induced Morphological Instability of Supported Polymethyl Methacrylate Thin Film"

1. Time evolution of PMMA bubbles in water.

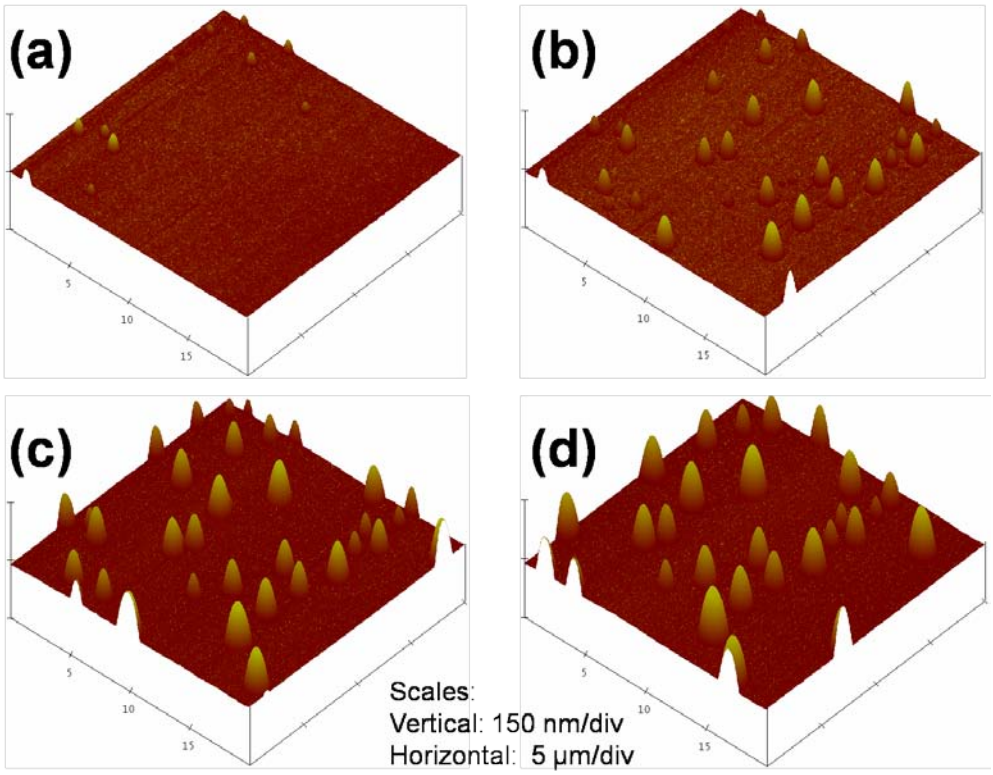

Figure 1S The time evolution of PMMA (M_w = 21.4 kg/mol) film morphology in water observed by *in-situ* AFM. The observation time is (a) 0 min, (b) 8 min, (c) 24 min, (d) 106 min, respectively. The thickness of PMMA film is 46 nm. The PMMA film was annealed at 60^{o}C for 24 h.

2. Effect of treatments on the morphology of PMMA film in water

Experiments have been conducted on PMMA films with different treatments, such as annealing temperature, annealing time, substrate surface treatment. The results (Figure 2S) show that such treatments affect the kinetics of the morphological evolution of the bubbles but do not affect their final dimension. As an example, the following data show the h and L and the fitting of R for three samples of same thickness but annealed at different temperatures (60, 80, and 90°C).

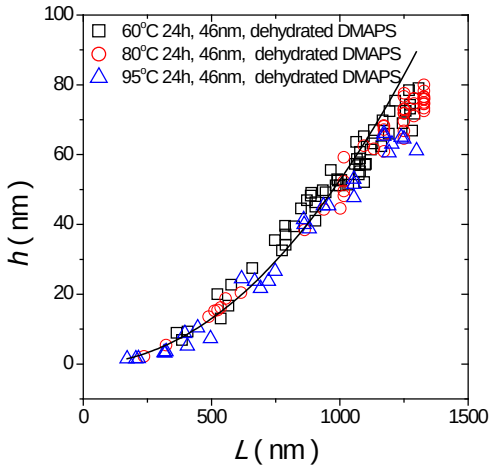

Figure 2S Dimension data of bubbles (*h* and *L*) in PMMA film samples with different annealing time. The solid line demonstrates the fitting of the radius of curvature (*R*) using the model of spherical cap for the bubbles, demonstrating the R value of ~3.3 μm.

3. Effect of annealing temperature on bubbles' number and area

The average foot-print area of single bubbles and average number of bubbles are investigated. Figure 3S indicated that both of parameters are only dependent on the annealing temperature. With the increasing of annealing temperature, the average foot-print area of single bubbles decreases while the average number of bubbles increases. These data show that the bubble formation is strongly dependent on the binding strength between film and substrates, as annealing enhances binding between film and substrates.

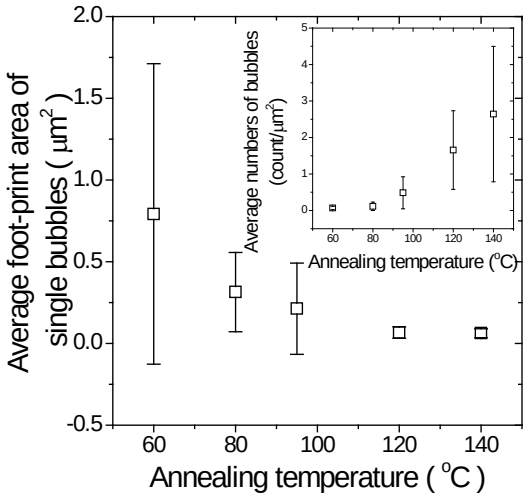

Figure 3S The effect of annealing temperature on the foot-print area of single PMMA bubbles in water. The insert is the effect of annealing temperature on the average numbers of bubbles. The thickness of PMMA film is 46 nm.

4. Theoretical analysis if water or vacuum is in the bubble

Case I: Water in the bubble

If water is in the bubble, there may exist another swollen layer beneath the interior layer, thus a three-layer (namely, outer swollen layer-interior layer-inner swollen layer) model should be used. Then the misfit between the inner swollen layer and the interior layer (which is due to swelling of water) is ε^*, and the misfit between the outer swollen layer and the interior layer is $-\varepsilon^*$. Similar to Eq. 4 in the paper, we can obtain the radius curvature of the bubble in this three-layer system. We assume that the thickness of the inner swollen layer is nearly the same as that for the outer swollen layer. The corresponding radius of curvature is shown in Figure 4S (dashed line). It shows that the three-layer model doesn't agree well with the experimental data as the two-layer model, indicating that the assumption of water inside the bubble is not reasonable.

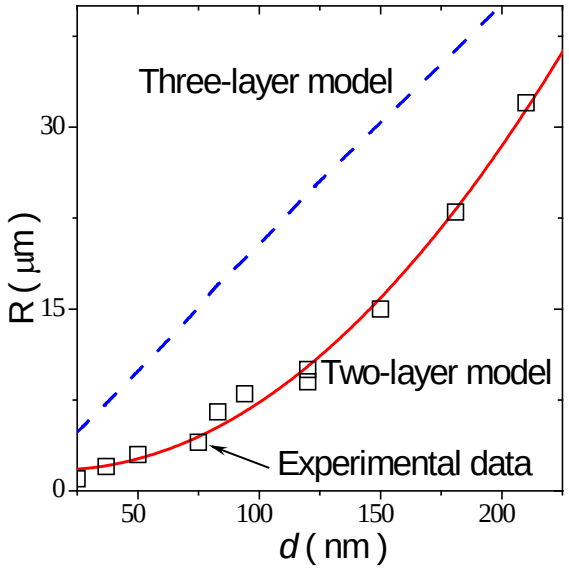

Figure 4S The radius of curvature of the bubbles as a function of the original thicknesses of the PMMA films. The dashed line is obtained from the three - layer model, the solid line is obtained from the theoretical model for two - layer system.

Case II: Vacuum in the bubble

If vacuum is in the bubble, the pressure difference (1 bar) between the exterior and interior regions of the bubble has a suppression effect on the PMMA film, namely, the pressure difference prevents the film from bubble formation, while the misfit is in favor of bubble formation. We establish the equilibrium equations for the bubbles under the pressure difference, misfit and interfacial tension. The result indicates that the effect of pressure difference is larger compared to those of the other two factors. In this case, the formation of bubble will never happen. Therefore, the assumption of

vacuum inside the bubble is not reasonable.

According to the analysis above and the result of the theoretical model with the presence of air in the paper, we believe that the space inside the bubbles is filled with air.